DYNAMICS OF MOTOR PROTEINS– A MONTE CARLO SIMULATION

A Thesis Submited in Partial Fulfillment of the
Requirments for the Degree of
Master of Science in Physics

Addis Ababa University
School of Graduate Studies

Asmamaw Asrat Demise
Addis Ababa, Ethiopia
July 2011

Addis Ababa University
School of Graduate Studies
College of Natural Sciences
Faculty of Chemical and Physical Sciences
Department of Physics

The undersigned hereby certify that they have read and recommend to the School of Graduate Studies for acceptance a thesis entitled "**Dynamics of Motor Proteins—A Monte Carlo Simulation**" by **Asmamaw Asrat Demise** in partial fulfillment of the requirements for the degree of **Master of Science in Physics**.

Dated: July 2011

Approved by the Examination Committee:

Dr. Tatek Yergou, Advisor ———————————

Dr. Mulugeta Bekele, Examiner ———————————

Dr. Lemi Demeyu, Examiner ———————————

ADDIS ABABA UNIVERSITY

Date: **July 2011**

Author: **Asmamaw Asrat Demise**

Title: **Dynamics of Motor Proteins—A Monte Carlo Simulation**

Department: **Department of Physics**

Degree: **M.Sc.** Convocation: **JULY** Year: **2011**

Permission is herewith granted to Addis Ababa University to circulate and to have copied for non-commercial purposes, at its discretion, the above title upon the request of individuals or institutions.

Signature of Author

'Biologists observe things that cannot be explained. Theorists explain things that cannot be observed'. Aharon Katchalsky

Table of Contents

List of Figures

Abstract

Motor proteins are mechanochemical enzymes that convert energy released by adenosine triphosphate (ATP) hydrolysis into either linear or rotary movement. Motor proteins: kinesin, myosin and dynein, that perform active movements along cytoskeletal filaments drive the long−range transport of vesicles, organelles, and other types of cargo in biological cells. In this Monte Carlo simulation study, based on the recent experimental results and existing theoretical models, a lattice model to study the dynamics of non−interacting motor proteins each transporting a cargo and a new bead−spring model to study the collective dynamics of interacting motor proteins transporting cooperatively a common cargo are proposed and studied.

Acknowledgements

It is a pleasure to acknowledge those who offered me their support and advice during my MSc studies. Such a list is necessarily incomplete, for which I apologize.

I would like to express my deep and sincere gratitude to my supervisor, Tatek Yergou. His wide knowledge and his logical way of thinking have been of great value for me. His understanding, encouraging and personal guidance have provided a good basis for the present thesis.

I warmly thank Mulugeta Bekele, for his valuable advice and friendly help.

I would like to thank Anatoly Kolomeisky, Stefan Klumpp, and Barak Gilboa, for their promptness in answering my questions and sending me important articles and links.

Finally, I could never have even started my thesis without the support of my family. For this, and so much more, they have my gratitude.

Chapter 1

Introduction

Organelles in cells are frequently transported distances of many micrometers along well–defined routes in the cytosol and delivered to particular intracellular locations. Diffusion alone cannot account for the rate, directionality, and destinations of such transport processes. For example, the high protein concentration (200–300 mg/ml) of the cytoplasm prevents organelles and vesicles from diffusing faster than 100 micrometers/3 hours [1, 2]. To generate the forces necessary for many cellular movements, cells depend on specialized enzymes commonly called molecular motors, or motor proteins. These mechanochemical enzymes convert the chemical energy derived from the hydrolysis of adenosine triphosphate (ATP) or contained within ion gradients into mechanical force, usually generating either linear or rotary motion [1, 2].

There are many different types of motor proteins, each specialized for a particular function [3]. Some move linearly along polymers (such as cytoskeletal and nucleic acid motor proteins), whereas others undergo rotary motions (such as rotary motor proteins). However, we consider here only linear cytoskeletal motor proteins. This is not inappropriate because many of the experimental and theoretical approaches to rotary and linear motor proteins have shown that the mechanisms these motors use to power cellular motility are essentially the same [2, 4].

1.1 Cytoskeletal motor proteins

Cytoskeletal motors that perform active movements along cytoskeletal filaments drive the long−range transport of vesicles, organelles, and other types of cargo in biological cells [5]. There are three classes of cytoskeletal motor proteins: myosins, kinesins and dyneins. Myosins move along actin filaments, and kinesins and dyneins move along microtubules.

In every case that hase been tested so far, myosins move toward the plus end of an actin filament−with one exception, myosin VI [2]. Kinesins (with the exception of kinesin 14 family members) move towards microtubule plus ends, whereas all dyneins discovered to date move towards microtubule minus ends [6].

Cytoskeletal motors have in common a highly conserved motor domain or "head", which consists of an ATP−binding/hydrolysis motif and an adjacent filament−binding region [7]. The "neck", a region that has been implicated in several aspects of motor function, lies between the motor domain and the coiled−coil dimerization domain (Fig. 1.1).

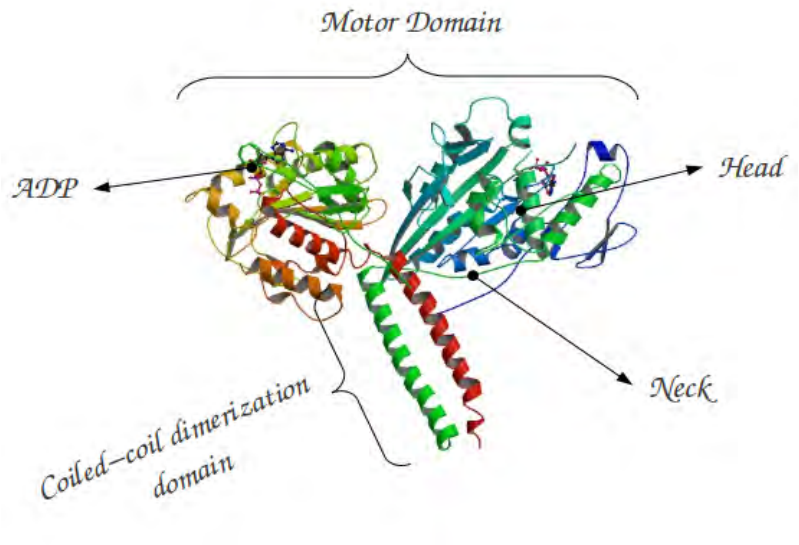

Figure 1.1: Crystal structure of dimeric kinesin [8].

These motors use a common principle to generate movement in which they bind to their track, undergo a force−producing conformational change (power stroke), release from the track, and then return to their original conformation (recovery stroke) [9, 10]. These structural changes are coupled to chemical transitions in the motors ATPase cycle: ATP binding, hydrolysis, and product release.

1.2 Single−molecule techniques

The study of motor proteins was revolutionized by the development of *in vitro* motility assays in which the motility of purified motor proteins along purified cytoskeletal filaments is reconstituted in cell−free conditions [2]. During the last decade, the properties of single processive motors, such as myosin V on actin filaments and kinesin on microtubules, have been characterized in some detail by using *in vitro* motility assays and novel single−molecule techniques, such as atomic force microscopy, single−molecule fluorescence microscopy and optical tweezers [5, 11].

Myosin molecules slide along actin filaments, fuelled by the chemical energy driven from ATP hydrolysis. The development of techniques for manipulation of a single actin filament and nanometry with a microneedle and optical tweezers has allowed individual mechanical events such as displacement and force to be measured from single molecules of myosin *in vitro* (see Fig. 1.2). A single myosin molecule has been found to generate mean displacements of 5 to 25 nm at nearly zero load and mean forces of 3 to 5 pN at high loads during a single ATP hydrolysis cycle [12]. The displacement records showed that the displacements do not take place in a single step but instead in several distinctive steps. The steps take place stochastically and some of them ($<\sim$ 10 % of total steps) were backward [12]. The step−size was 5.5 nm, coinciding with the interval between adjacent monomers in one strand of an actin filament. Taking all these results into account, a new

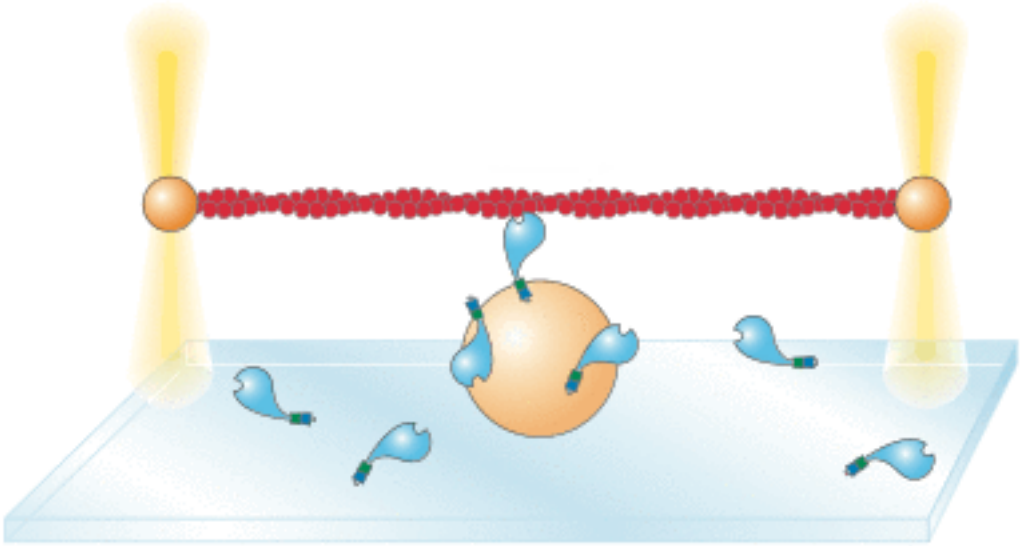

Figure 1.2: Optical tweezer determines the step size and force of a single myosin molecule [1].

model has been proposed that suggests a myosin head can walk on actin monomers in its filament by Brownian motion, biased Brownian ratchet model. This model challenges a currently accepted model, the so called "lever−arm swinging model", in which the neck region of a myosin head swings relative to the main body of the head to generate force and displacement, and the swing motion is coupled tightly to the ATP hydrolysis cycle in a one to one fashion. In the lever−arm swinging model, the myosin molecule moves in a single step. In the biased Brownian ratchet model, movement of myosin is driven by the Brownian motion and unidirectional movement is produced by rectification of thermal fluctuations induced by the conformational change in the motor caused by ATP hydrolysis [12, 13].

On average a single kinesin molecule moves along the surface of a microtubule through a distance of 5 μm in microtubule gliding assays, 1.4 μm in bead assays, and 0.6−1.3 μm in fluorescence assays [14]. A single kinesin molecule exhibits a stepwise displacement with amplitude of 8 nm by hydrolysis of one ATP molecule [12]. An 8 nm step reflects the periodicity of the tubulin heterodimers in a microtubule. Based on

this finding, a hand−over−hand model has been proposed, in which a kinesin walks on tubulin heterodimers via its two heads in an alternating fashion. Because the movement takes place in 8 nm steps, the spacing of the adjacent tubulin dimers that form kinesins consecutive binding sites, and because each step is associated with one cycle of ATP hydrolysis, kinesin is expected to hydrolyze some 80−600 ATP molecules before it dissociates from the microtubule [14]. These observations show that the probability of kinesin dissociating during any one ATP hydrolysis cycle is only $\sim 1\%$. Because kinesin remains processive even against high loads of up to several piconewtons, kinesin must spend <1 μs in a detached state per hydrolysis cycle, and it is likely that kinesin maintains continuous attachment to the microtubule [14]. Single molecules of the kinesin super−family and mutant kinesin molecules which are one−headed, have also shown continuous movement along a microtubule although the travel distance was smaller. The motion was not smooth and the direction fluctuated in forward and backward directions [12]. Thus, as for myosin, Brownian motion appears to play an essential role in this movement.

Unlike kinesin, relatively little is known about the molecular mechanism of dynein. Single−molecule studies suggest that dynein walks in a hand−over−hand−like fashion, although its stepping behavior and directionality are more irregular than kinesin's. Evidence has shown that dynein advances via coordination of its two motor domains, but the details of cytoplasmic dynein's step size, stall force, and directionality remain controversial. Observations of variable step sizes (4−32 nm) and directionality suggest a considerable diffusional component to its step, making dynein stepping more akin to that of myosin VI (21−51 nm) than kinesin [15]. A $\sim$10 nm long linker that connects the ATPase domain to the tail binding domain has been suggested to power dynein motion [15]. The linker shifts its position relative to the catalytic ring during the ATPase cycle and is believed to facilitate dynein motility. However, with no atomic structure for dynein in hand, a structural model for dyneins motility is less advanced than that for kinesin.

1.3 Models

Many cellular processes such as cellular transport, organization, and function require the cooperative work of many motors in order to preserve persistent motion and force generation [16]. For example, active cellular transport, such as organelle traffic, is driven by motor proteins of different families such as kinesin, myosin, and cytoplasmic dynein (Fig. 1.3) [17]. From a theoretical point of view, cooperative dynamics of molecular motors have been investigated using several distinct models. These models include: (1) Transition Rate Model, and (2) Two−state Ratchet Model [5, 16, 18, 19]. In this section we discuss the foundations of these models.

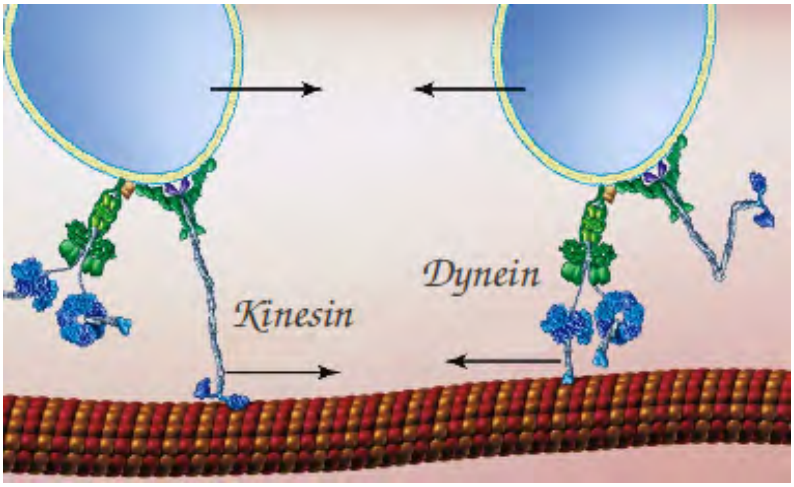

Figure 1.3: Cooperative work of kinesin and dynein [20].

1.3.1 Transition rate model

The model considers cargo particles that are transported by N motors. These motors are firmly attached to the cargo particle but can bind to and unbind from the filament along which they move. Thus, the number n of motor molecules that are bound to the filament can vary between $n = 0$ and $n = N$. If the cargo particle is linked to the filament through n motors, it moves with velocity v_n. Unbinding of a motor from the filament and binding

of an additional motor to the filament occur with rates ε_n and π_n, respectively (Fig. 1.4). All these quantities can be directly measured by particle tracking both *in vivo* and *in vitro*.

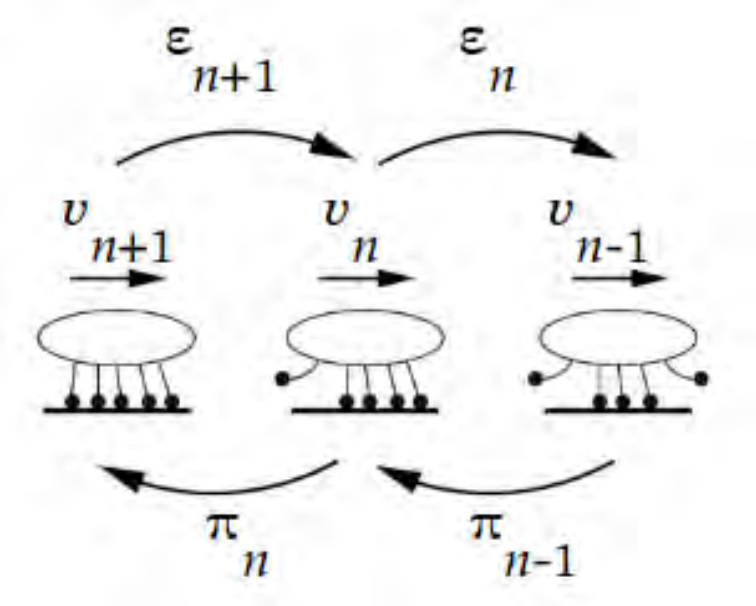

Figure 1.4: Transition rate model. A cargo particle is transported cooperatively by n motor proteins.

We denote by P_n the probability that the cargo particle is in state $|n\rangle$, i.e., bound to the filament by n motors. These probabilities satisfy the master equation

$$\frac{\partial}{\partial t}P_n = \varepsilon_{n+1}P_{n+1} + \pi_{n-1}P_{n-1} - (\varepsilon_n + \pi_n)P_n. \tag{1.3.1}$$

To determine the transport properties of the bound cargo particles, we need to have the distribution of the bound motors. Using the stationary solution of the master equation,

$$\frac{\partial}{\partial t}P_n = 0. \tag{1.3.2}$$

Which is,

$$\varepsilon_{n+1}P_{n+1} = \pi_n P_n, \tag{1.3.3}$$

for $0 \leq n \leq N-1$. And, the normalization condition

$$\sum_{n=0}^{N} P_n = 1. \tag{1.3.4}$$

we can have the distribution of the number of bound motors,

$$P_0 = \left[1 + \sum_{n=0}^{N-1} \prod_{i=0}^{n} \frac{\pi_i}{\varepsilon_{i+1}}\right]^{-1} \quad \text{and} \quad P_n = P_0 \prod_{i=0}^{n-1} \frac{\pi_i}{\varepsilon_{i+1}}. \tag{1.3.5}$$

Using this distribution the model determines the transport properties of the bound cargo particles.

1.3.2 Two−state ratchet model

The model considers the one−dimensional motion of a group of N point particles (representing the motors) connected (mechanically coupled) to a rigid rod with equal spacing q (see Fig. 1.5). The cytoskeletal track is represented by a periodic saw−tooth potential, $U(x)$, with period l and height H. The model requires that q is larger than and incommensurate with l. The motors are identical and walk on a track which is globally apolar and, thus, does not permit net transport to the right or left over large time scales. The temporal direction of motion is determined by the net force generated by all the motors. The local polarity of the track is represented by an additional force of size f_{rand} which, within each unit of the periodic potential, points to the right or to the left. The globally apolar nature of the track is ensured by requiring that the sum of these random forces vanishes.

The instantaneous force between the track and the motors is given by the sum of all the forces acting on the individual motors:

$$F_{tot} = \sum_{i=1}^{N} f_i^{motor} = \sum_{i=1}^{N} \left[-\frac{\partial U(x_1 + (i-1)q)}{\partial x} + f_{rand}(x_1 + (i-1)q)\right].C_i(t), \tag{1.3.6}$$

where $x_1 + (i-1)q$ is the coordinate of the ith motor.

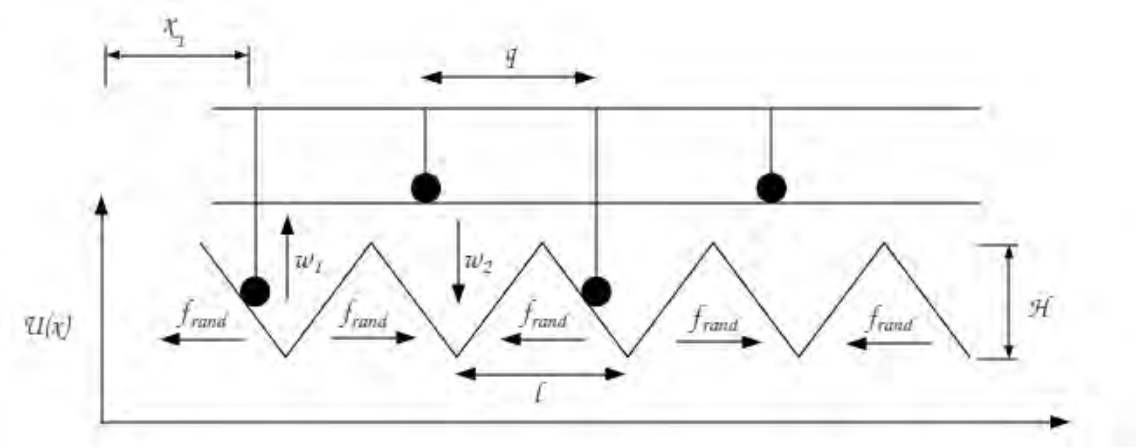

Figure 1.5: Two−state ratchet model. N point particles (representing the motors) are connected to a rigid rod with equal mean spacing q.

The two terms in the square brackets represent the forces due to the symmetric saw−tooth potential and the additional random local forces acting in each periodic unit. The function $C_i(t)$ takes two possible values, 0 or 1, depending on whether the motor i is detached from or attached to the track, respectively, at time t. The motors change their binding states ($|0\rangle$: detached; $|1\rangle$: attached) independently of each other. If an attached motor is located in one of the regions centered around the potential minima, the motor may become detached ($|1\rangle \rightarrow |0\rangle$) with a probability per unit time ω_1. Conversely, a detached motor may attach to the track ($|0\rangle \rightarrow |1\rangle$) with transition rate ω_2.

At each instance, the group velocity of the motors is proportional to the total force exerted by the motors (see Eq. 1.3.6),

$$v(t) = F_{tot}(t)/\lambda, \tag{1.3.7}$$

where the friction coefficient, λ, depends mainly on motors attached to the track, $N_c \leq N$ at time t: $\lambda = \lambda_0 N_c$.

Chapter 2

Models and Methods

In this Monte Carlo simulation study, we first investigate the dynamics of motor proteins each transporting a cargo, and we then investigate the dynamics of motor proteins transporting cooperatively a common cargo. In the first section of this chapter, we discuss the foundations of Monte Carlo method. The discussion is based primarily on references [21], [22], and [23]. In subsequent sections, we present a model for each investigation in detail.

2.1 Monte Carlo method

The Monte Carlo method was developed by von Neumann, Ulam, and Metropolis at the end of the Second World War to study the diffusion of neutrons in fissionable material. The name "Monte Carlo", chosen because of the extensive use of random numbers in the calculation, was coined by Metropolis in 1947 and used in the title of a paper describing the early work at Los Alamos laboratory [24].

Up to now the approach to computing properties of physical systems has been to use the fundamental equations of motion to generate paths in phase space. The quantity of interest has then been evaluated along this path. That the quantity thus obtained is indeed equal to the ensemble average is ensured by the fundamental relation, i.e., that

the trajectory averages are equal to ensemble averages. The Monte Carlo (MC) method in simulational physics takes a different approach. It starts out with a description of the system in terms of a Hamiltonian, and an appropriate ensemble for the problem is selected. Then all observations are computable using the associated distribution function and the partition function. The idea is to sample the main contribution to get an estimate for the observable. The MC technique in statistical physics is centered around the computation of mathematical expectations. Ultimately the goal is to compute quantities appearing as results of high dimensional integrations.

The MC method gives information on the configurational properties, in contrast to the molecular dynamics (MD) which yields the true dynamics. The MD method gives information about the time dependence and the magnitude of position and momentum variables. By choosing an appropriate ensemble, like the canonical ensemble, the MC method can evaluate observables at a fixed particle number, volume and temperature. The great advantage of the MC method is that many ensembles can be quite easily realized, and it is also possible to change ensembles during a simulation.

At first glance one would say that the MC method performs an ensemble average. However, it has been recognized that actually a time average is performed in the course of a MC simulation, similar to the one in MD; only here the trajectory runs through configurational space, whereas the trajectory in molecular dynamics runs through the position−momentum space.

Because of limits on computer speed there are some problems which are inherently not suited to computer simulation, at this time. A simulation which requires years of CPU time on whatever machine is available is simply impractical. Similarly a calculation which requires memory which far exceeds that which is available can be carried out only by using very sophisticated programming techniques which slow down running speeds and greatly increase the probability of errors. It is therefore important that the user first

consider the requirements of both memory and CPU time before embarking on a project to ascertain whether or not there is a realistic possibility of obtaining the resources to simulate a problem properly.

2.2 Motor proteins each transporting a cargo

To study the dynamics of non−interacting motor proteins each transporting a cargo, we propose a lattice model based on the model discussed by R. Lipowsky *et al.* in [25]. In this model, each motor performs directed movement along a filament and unbinds from it after a certain walking distance. The unbound motor diffuses in the surrounding fluid until it rebinds to the filament and resumes directed motion.

2.2.1 Simulation algorithm

We consider a two dimensional lattice of size L_X along x and L_Y along y with lattice constant L, corresponding to the spacing of the adjacent binding sites. Each lattice site is labeled with integer coordinates (n, m). We represent the track: the protofilament of the filament, with the lattice sites $(n, L_Y/2)$ (see Fig. 2.1).

We start our simulation by putting ATP molecules of concentration ρ and N motor proteins randomly on the lattice. Each ATP molecule can diffuse freely to one of its four nearest neighbor lattice points if it is empty.

At filament sites $(n, L_Y/2)$, if a motor gets ATP molecule, the motor will hydrolyse the ATP with ATP−intake probability p to step forward from $(n, L_Y/2)$ to $(n+1, L_Y/2)$. In order for a given motor to hydrolyse an ATP molecule the latter has to be in the vicinity of the motor. In the present model we consider an ATP molecule to be in the immediate neighborhood of a motor if they share the same lattice site. To keep the number of ATP

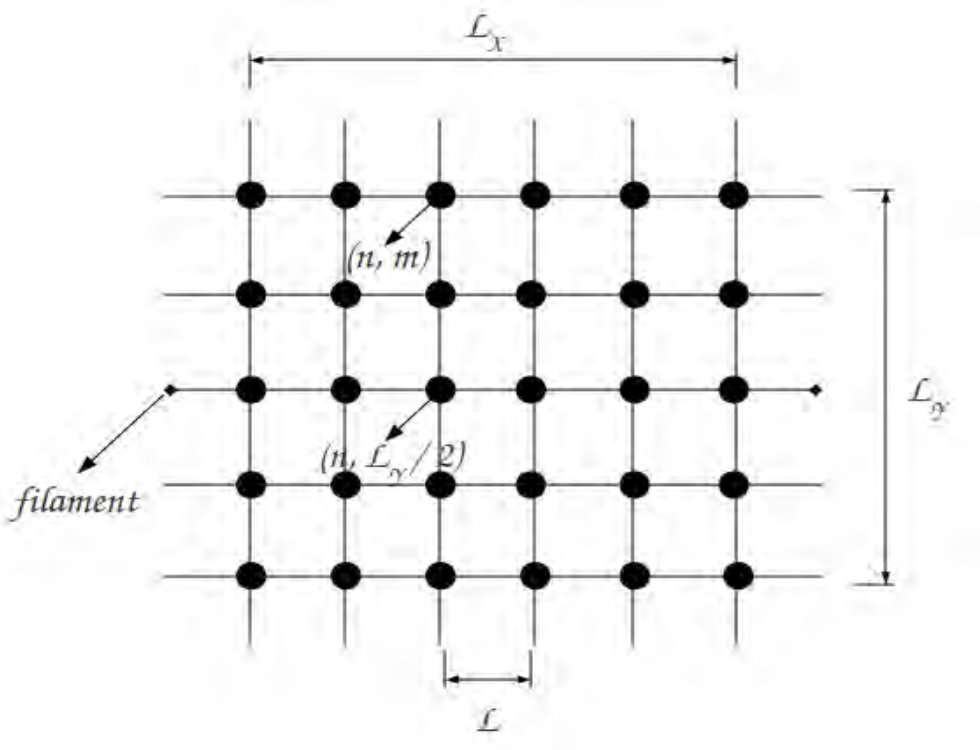

Figure 2.1: Schematic representation of the lattice points.

molecules constant, we update the ATP concentration ρ for each motor forward step. If the motor is not able to hydrolyse the ATP, then the motor will stay on the filament $(n, L_Y/2)$ waiting for ATP molecule to bind with a probability w or will detach from the filament: the motor will move either to $(n, L_Y/2+1)$ or $(n, L_Y/2-1)$, with a probability d. In the absence of ATP molecule, the motor will stay on the track $(n, L_Y/2)$ with the probability w or will perform free diffusion: the motor will detach with the probability d from or slide with a probability s on the filament [26, 27].

Any detached motor protein from the track performs free Brownian motion without hydrolysing ATP in the surrounding fluid: detached motor can diffuse freely to one of its four nearest neighbor lattice points with equal probability if it is empty.

2.3 Motor proteins transporting a common cargo

Based on the recent experimental results and existing theoretical models, we propose a new bead−spring model for interacting motor proteins transporting cooperatively a common cargo [18, 28, 29, 30, 31, 32]. We considered the two−state model: the surface potential felt by the motors alternates between asymmetric sawtooth potential profile (on state), $U(x)$, with period l (filament period) and height H (binding energy), and a flat profile (off state) along which the motors can diffuse freely. The switching from one profile to the other is controlled by ATP hydrolysis and product release. Each motor protein i works independently as does a locomotive and interact to its nearest neighbor motor j through the cargo as if they are connected with a spring of length q_{ij} and stiffnes k_{ij}, and switch from on state to off state and vice versa with a rate ω_i and ν_i respectively. The model requires that q_{ij} is larger than and incommensurate with l (Fig. 2.2).

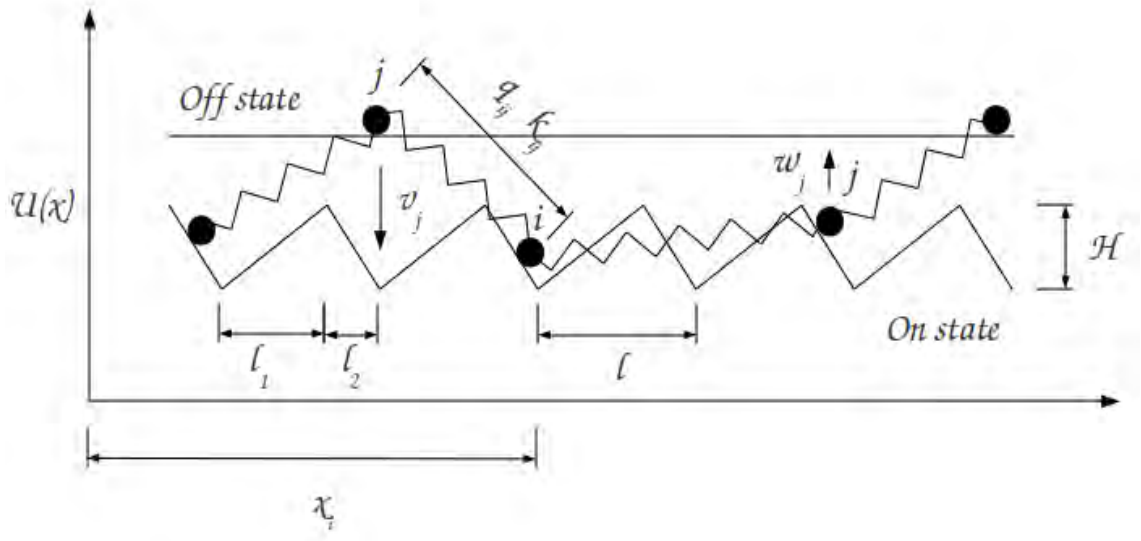

Figure 2.2: Bead−spring model. Interacting motor proteins transporting cooperatively a common cargo.

2.3.1 Simulation algorithm

To study the dynamics of interacting motor proteins that are transporting cooperatively on a filament and irreversibly attached to a common cargo, we consider a one−dimensional lattice of length L with lattice constant l, corresponding to the period of the saw−tooth potential.

We start our simulation by setting N motor proteins randomly on the filament (lattice): a motor protein i can be either in on state or off state with a probability ν_i or ω_i respectively. To move a randomly chosen motor protein, we then implement the Metropolis algorithm that is presented by N. Metropolis *et al.* in [33]. The algorithm is:

1. Select a motor protein i randomly, and calculate its current total energy E, which is
$$E = U(x_i) + \frac{1}{2}k_{ij}\delta x^2|_{j=i-1} + \frac{1}{2}k_{ij}\delta x^2|_{j=i+1},$$
where $\frac{1}{2}k_{ij}\delta x^2|_j$ is the elastic interaction energy of neighbor motor j.

2. Make a random trial move, and calculate its current total energy $E^{'}$, which is
$$E^{'} = U(x_i^{'}) + \frac{1}{2}k_{ij}\delta x^{'2}|_{j=i-1} + \frac{1}{2}k_{ij}\delta x^{'2}|_{j=i+1}.$$
where $x_i^{'} = x_i + \delta$, $\delta x^{'2}|_{j=i-1} = (\delta x \pm \delta)^2\,|_{j=i-1}$, and $\delta x^{'2}|_{j=i+1} = (\delta x \mp \delta)^2\,|_{j=i+1}$.

3. If $E^{'} < E$, then accept the move and go to step 1. Else, generate a random number p between 0 and 1, and if $p < exp(E - E^{'})$, then accept the move and go to step 1. Otherwise, reject the move and go to step 1.

Chapter 3

Results and Discussions

The outline of this chapter is the following. In the first section of this chapter, we present and discuss results for a motor protein transporting a cargo. Following this section, we present results and discuss their implications for interacting motor proteins transporting cooperatively a common cargo.

3.1 A motor protein transporting a cargo

Motor proteins are often classified according to their processivity [34]. Processive motor proteins rarely detach from the track on which they are moving; they perform best when working in small groups and are therefore referred to as "porters". Nonprocessive motor proteins detach from the track frequently; they work best in large groups and are referred to as "rowers". An example of a porter is kinesin−1 which can move continuously along the surface of a microtubule for up to several microns, while muscle myosin II which move along actin filaments is an example of a rower [2].

To understand motor proteins processivity using the model that we discussed in the previous chapter for non−interacting motor proteins, we have calculated Hurst exponents, forward−backward step ratios, and dwell−time and run−length distributions of a motor protein transporting a cargo along its track for different ATP concentrations

ρ and ATP−intake probabilities p. In our simulation, we used the values 1000, 10, and 1 for L_X, L_Y, and L respectively, and each probability i.e. w, d, and s are equal (see Fig.2.1).

3.1.1 Hurst exponent

The Hurst exponent provides an index of whether a system is controlled by a truly random process or if there are underlying trends that create short−or long−term correlations over time among values. The following interpretations hold for different values of the Hurst exponent H:

- $H = 0.5$ applies to true random Brownian motion, uncorrelated.
- $0.5 < H < 1$ applies to fractal Brownian motion, showing a positive correlation (an increase is likely to be followed by an increase, a decrease in value by a decrease etc.), called persistent.
- $0 < H < 0.5$ applies to fractal Brownian motion, showing a negative correlation, called anti−persistence.

To investigate the correlations of successive motor steps, we have calculated Hurst exponent H dependence on ATP−intake probabilities p and ATP concentrations ρ using the relation,

$$\langle r^2 \rangle \sim t^{2H}. \tag{3.1.1}$$

Fig. 3.1 shows that the dependence of Hurst exponent H on ATP−intake probability p for three typical ATP concentration ρ whereas Fig. 3.2 depicts the variation of Hurst exponent H as a function of ATP concentration ρ for low, intermediate and high ATP−intake probability p. These plots show that for low ATP concentrations ρ or/and ATP−intake

probabilities p, the values of the Hurst exponent H are about 0.5, indicating that the motor performs random Brownian motion. Hurst exponent H dependence on ATP−intake probability p for intermediate ATP concentrations ρ (Fig. 3.1), and on ATP concentration ρ for intermediate ATP−intake probabilities p (see Fig. 3.2) show a linear growing trend. However, for high ATP concentrations ρ (Fig. 3.1), and high ATP−intake probabilities p (see Fig. 3.2) show a change in slope.

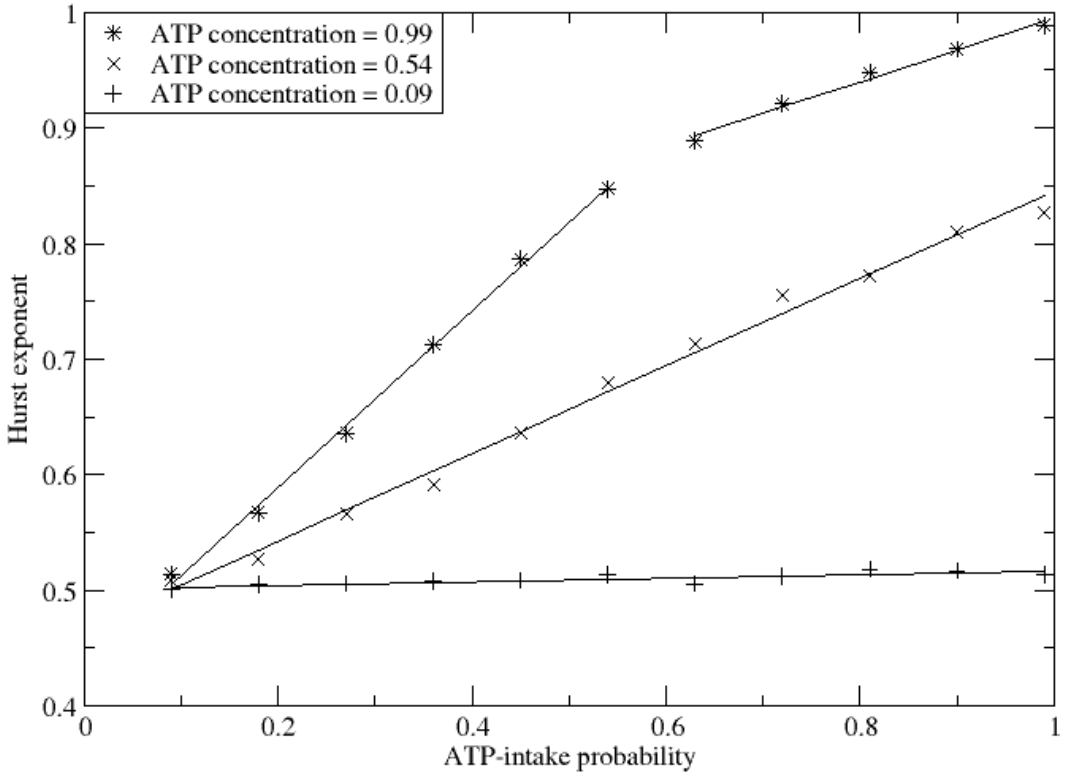

Figure 3.1: Hurst exponent H vs. ATP−intake probability p for low, intermediate, and high ATP concentrations ρ. Where the trend lines are plotted to show the change in slope.

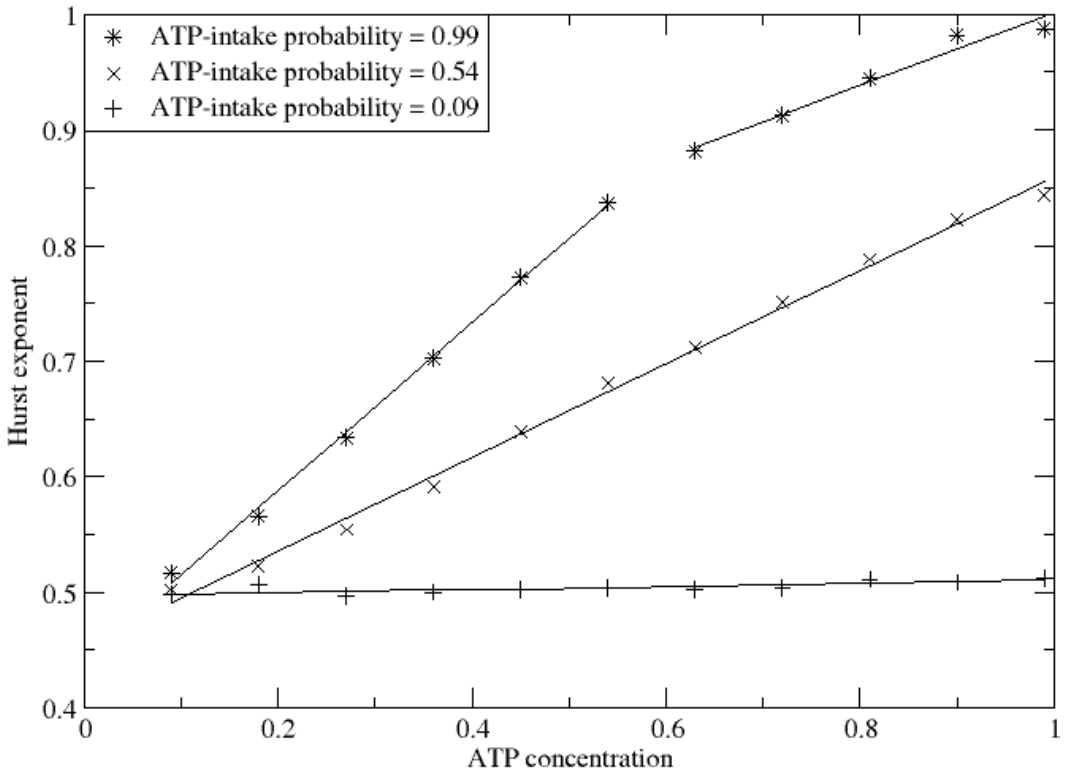

Figure 3.2: Hurst exponent H vs. ATP concentration ρ for low, intermediate, and high ATP−intake probabilities p. Where the trend lines are plotted to show the change in slope.

3.1.2 Forward−backward step ratio

To understand the transition between the forward and backward motions, we have calculated forward to backward step ratios n_+/n_- for different ATP concentrations ρ and ATP−intake probabilities p while the motor is moving on the filament. The forward to backward step ratio n_+/n_- takes three typical ranges of values corresponding to different scenario:

- $\frac{n_+}{n_-} = 1$ which implies random walk: the number of forward and backward steps are equal.
- $\frac{n_+}{n_-} \gg 1$ which indicates biased motion to the right (forward).
- $\frac{n_+}{n_-} \sim 0$ which points out biased motion to the left (backward).

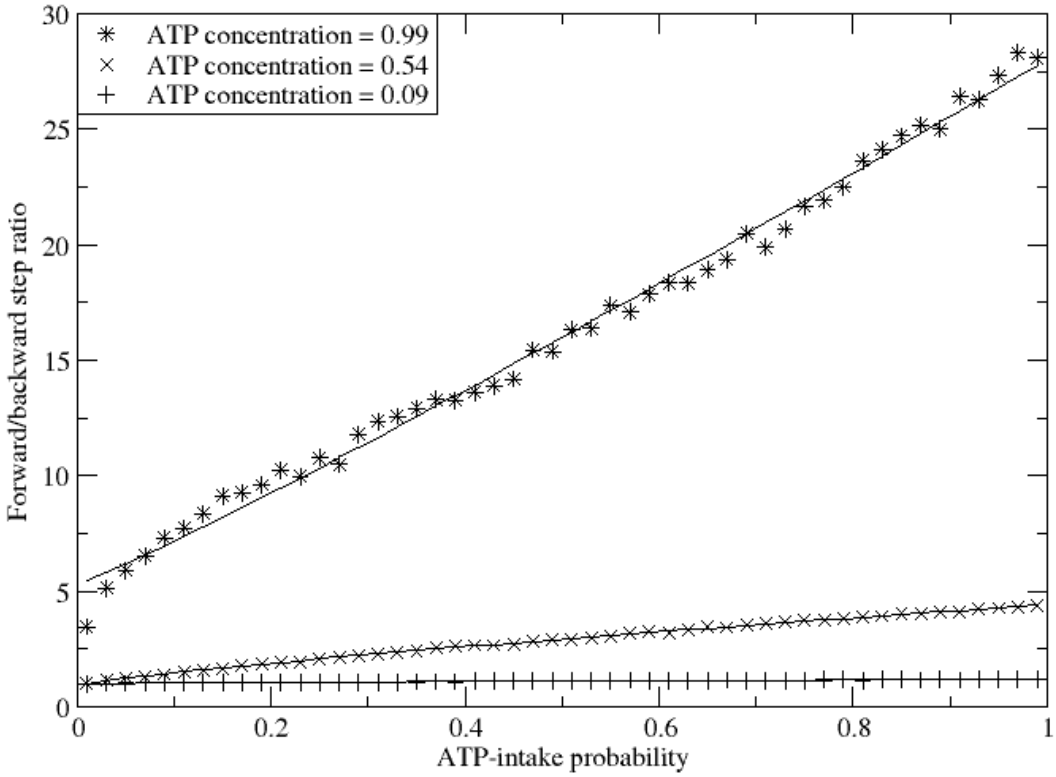

Figure 3.3: Forward/backward step ratio vs. ATP−intake probability p for high, intermediate, and low ATP concentrations ρ. Where the lines are plotted to show the linear dependence of H.

We first studied dependency of the ratio on ATP−intake probability p for low, intermediate, and high ATP concentrations ρ (see Fig. 3.3). As seen from Fig. 3.3, there

is a linear dependency between forward/backward step ratio n_+/n_- and ATP−intake probability p. Which is evident because the active movement of motor proteins is powered by ATP hydrolysis. This ratio becomes unity for low ATP concentrations ρ: the motor performs free diffusion. We also studied its dependency on ATP concentration ρ for different values of ATP−intake probabilities p (see Fig. 3.4). In contrast to the linear dependence seen in Fig. 3.3, Fig. 3.4 shows neither linear nor power−law dependence of the forward/backward step ratio n_+/n_- on ATP concentration ρ.

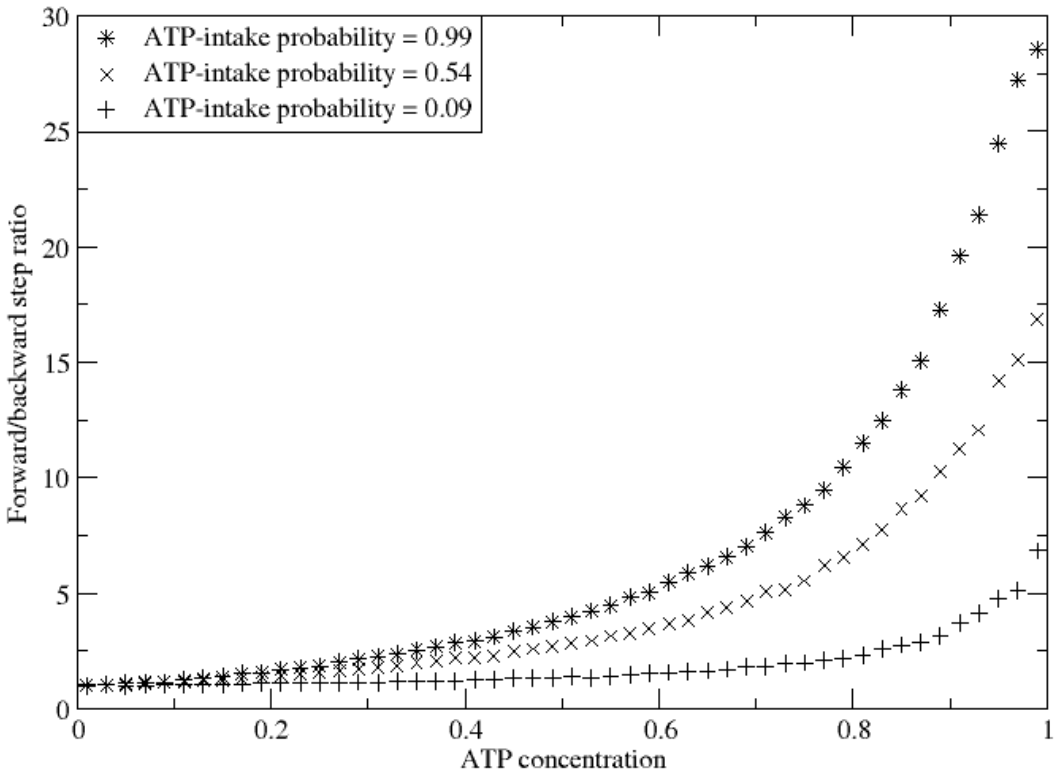

Figure 3.4: Forward/backward step ratio vs. ATP concentration ρ for low, intermediate, and high ATP−intake probabilities p.

3.1.3 Dwell−time and run−length distribution

We have also investigated two quantities of interest that is, the dwell−time t and the run−length l. The dwell−time t is defined as the time length spent by the motor on the filament without being detached from it, whereas the run−length corresponds to the algebraic distance traveled by the motor without changing direction. Distance traveled in the right direction is considered as positive while distance traveled in the left direction is considered as negative. Fig. 3.5−3.16 depict the distributions of dwell−times as well as run−lengths for different values of ATP concentration ρ, and ATP−intake probability p.

- Low ATP concentration (Fig. 3.5 and 3.6)

  Fig. 3.5 show dwell−time distributions for $\rho = 0.09$ and for different values of the ATP intake probability (from $p = 0.09$ up to $p = 0.99$). All the curves are almost identical and are exponentially decreasing functions of p. The fact that they are all similar implies that the dwell−time is insensitive to the intake probability in the limit of low concentration. For that case, the motion of the motor is essentially a random walk. The fit with an exponentially decaying function yields a mean characteristic dwell−time $\tau_c = 1.98$. The distributions of run−lengths are also independent of p and present the characteristics of a Gaussian distributions a very peculiar property of random walks.

- Intermediate ATP concentration (Fig. 3.7 and 3.8)

  At intermediate ATP concentration ($\rho = 0.54$), the dwell−time distributions are still an exponentially decaying functions of p, but depend now upon p, a fact that is evidenced by the increasing tail of the distributions as p tends towards 1. As a consequence, the characteristic times τ_c depend upon the intake probability and are increasing functions of p. This observation is corroborated by the distributions of run−length which present skewed right tails for large p.

- High ATP concentration (Fig. 3.9 and 3.10)

  The observed increase of the tails of the dwell−time distributions becomes more obvious for high ATP concentration, as depicted in Fig. 3.9. For instance, the probability for the motor to stay on the filament for times greater than 50 Monte Carlo time step (MCS) is non−zero when $p = 0.99$. The characteristics times take large value up to $\tau_c = 13.374$. As for the run−length distributions (Fig. 3.10), they represent fat tails in a more pronounced fashion. In particular when both ρ and p tend towards 1, the dominant motion mechanism is the directed movement. Since we have assumed that the motor moves at constant velocity, $l \sim t$, therefore the right sides of the distributions should have the same functional form as the dwell−time distributions which are found to be an exponential decay.

- Low ATP−intake probability (Fig. 3.11 and 3.12)

- Intermediate ATP−intake probability (Fig. 3.13 and 3.14)

- High ATP−intake probability (Fig. 3.15 and 3.16)

The results obtained for the last three cases are very similar to the former three cases respectively and so are their analysis.

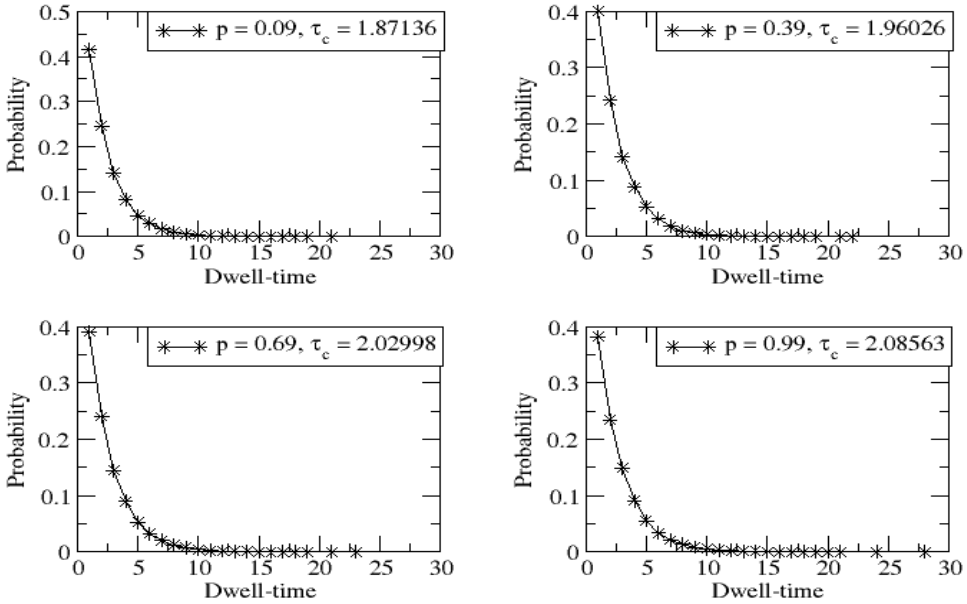

Figure 3.5: Dwell−time distribution with ATP concentration $\rho = 0.09$.

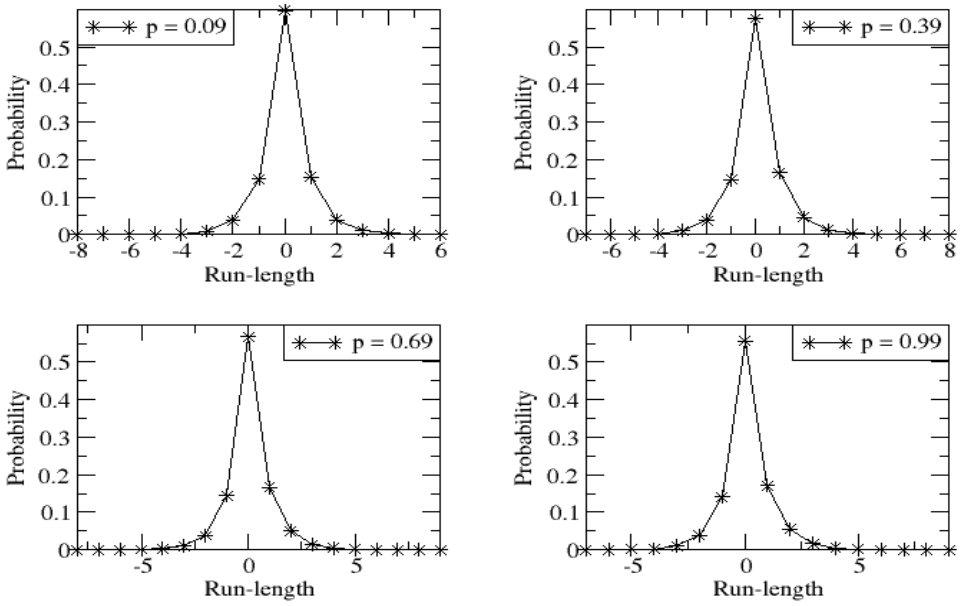

Figure 3.6: Run−length distribution with ATP concentration $\rho = 0.09$.

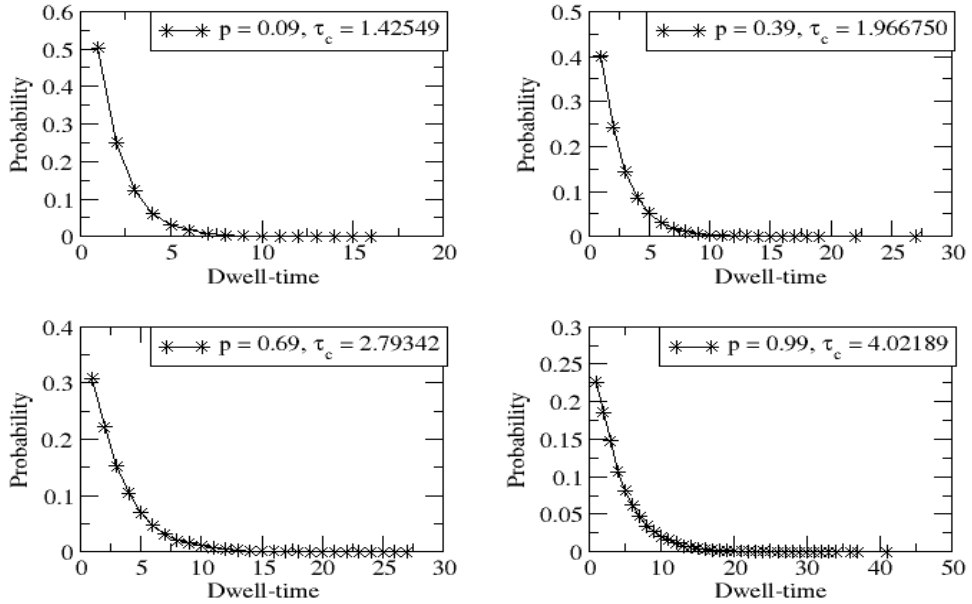

Figure 3.7: Dwell−time distribution with ATP concentration $\rho = 0.54$.

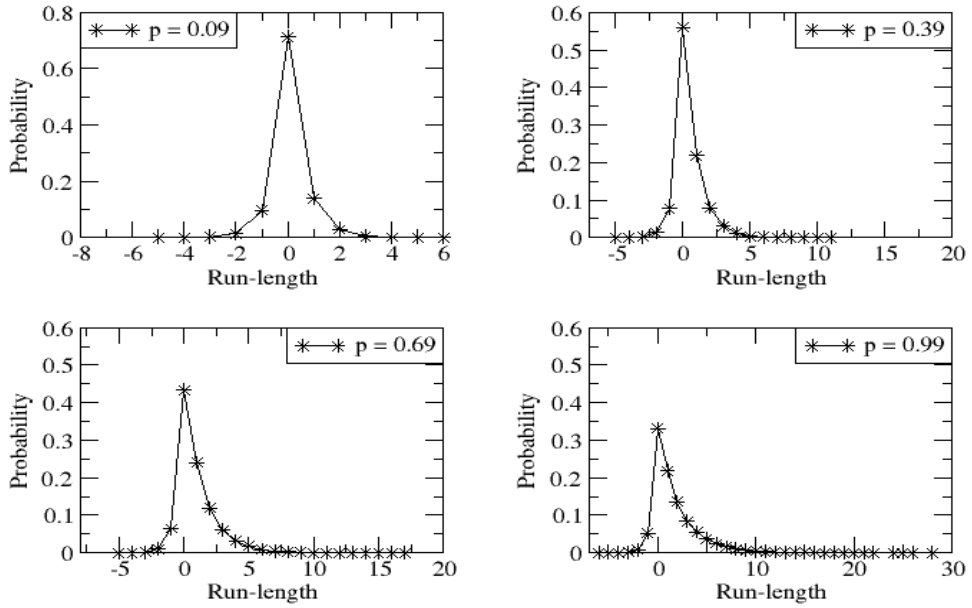

Figure 3.8: Run−length distribution with ATP concentration $\rho = 0.54$.

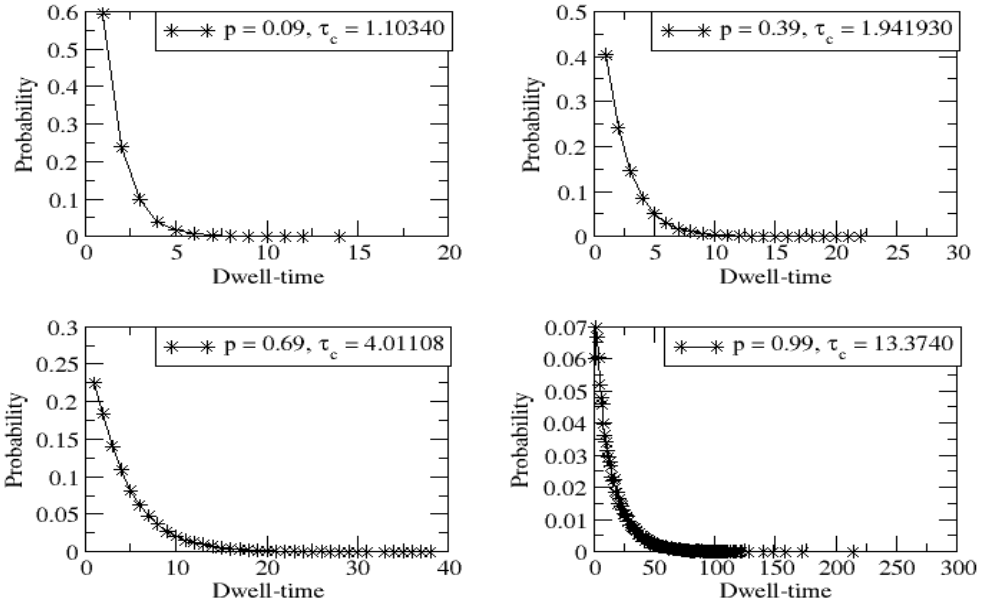

Figure 3.9: Dwell−time distribution with ATP concentration $\rho = 0.99$.

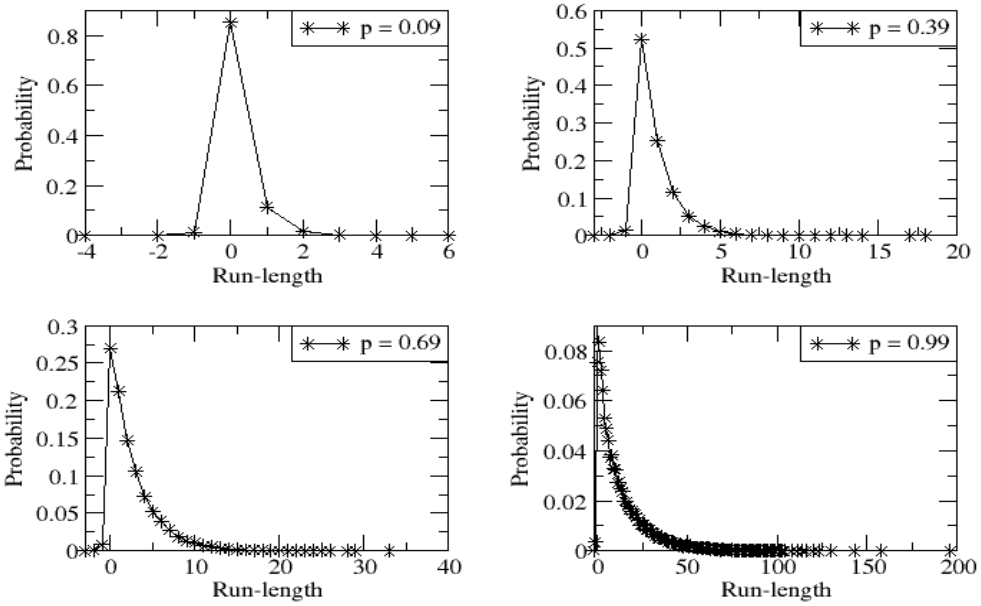

Figure 3.10: Run−length distribution with ATP concentration $\rho = 0.99$.

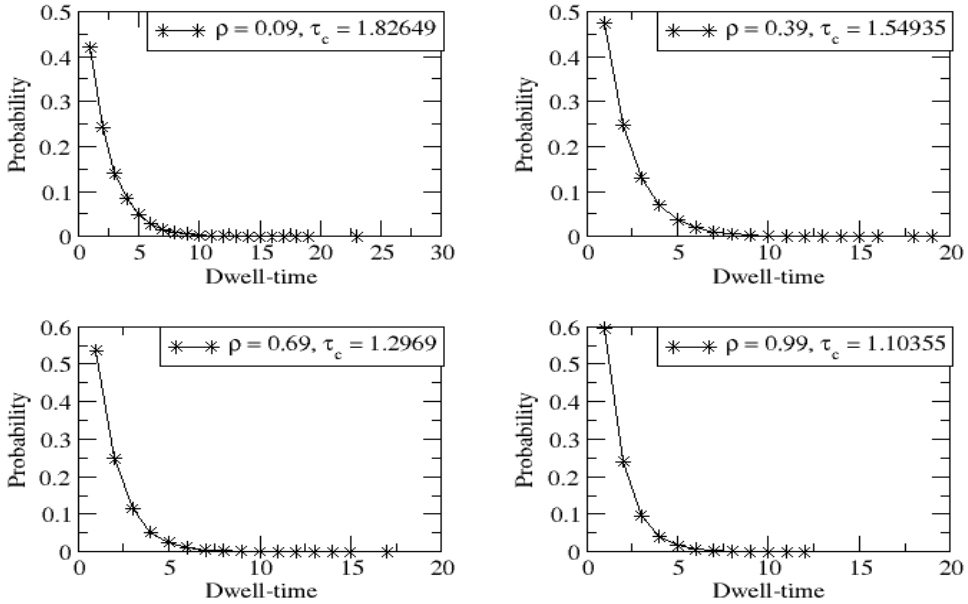

Figure 3.11: Dwell−time distribution with ATP−intake probability $p = 0.09$.

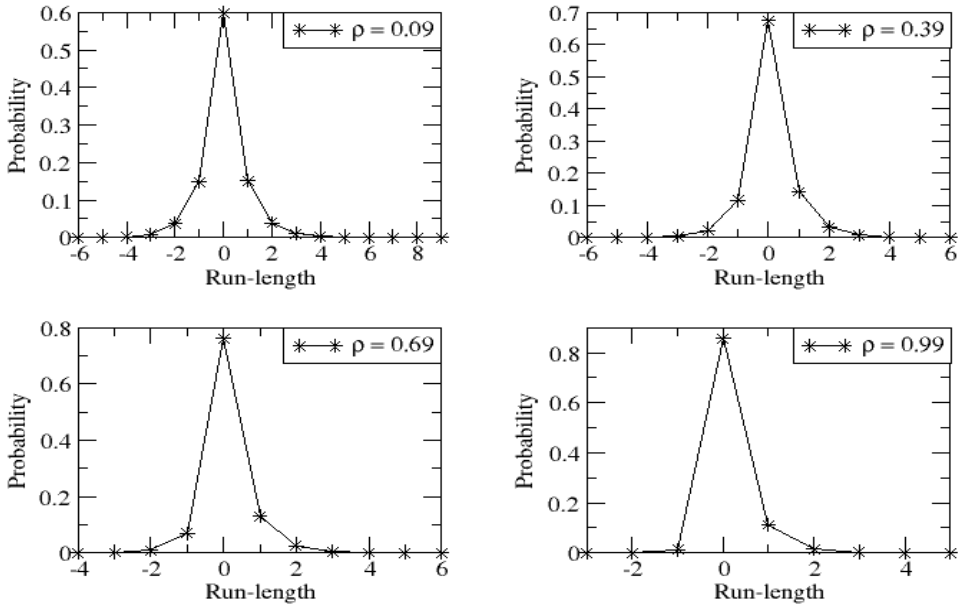

Figure 3.12: Run−length distribution with ATP−intake probability $p = 0.09$.

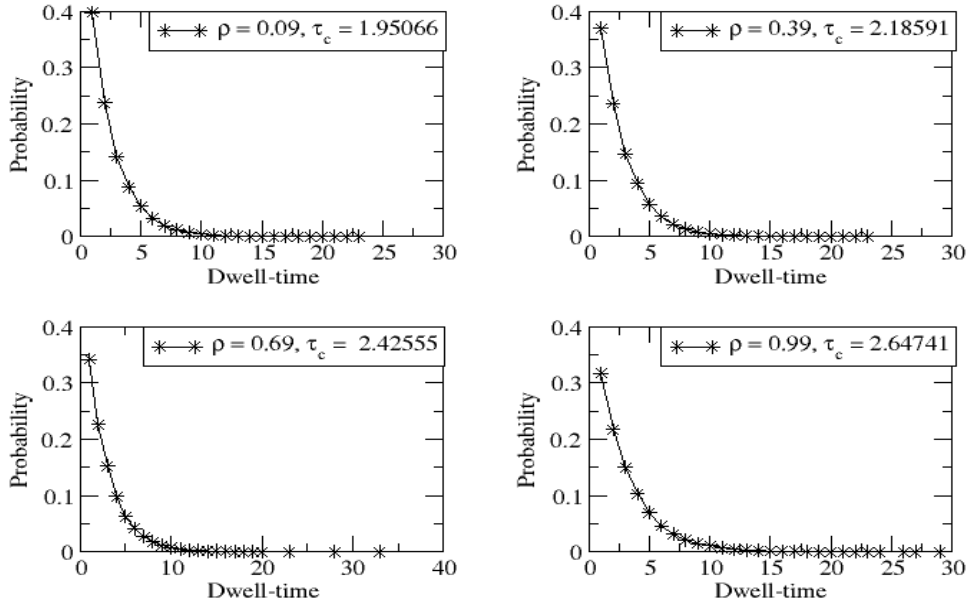

Figure 3.13: Dwell−time distribution with ATP−intake probability $p = 0.54$.

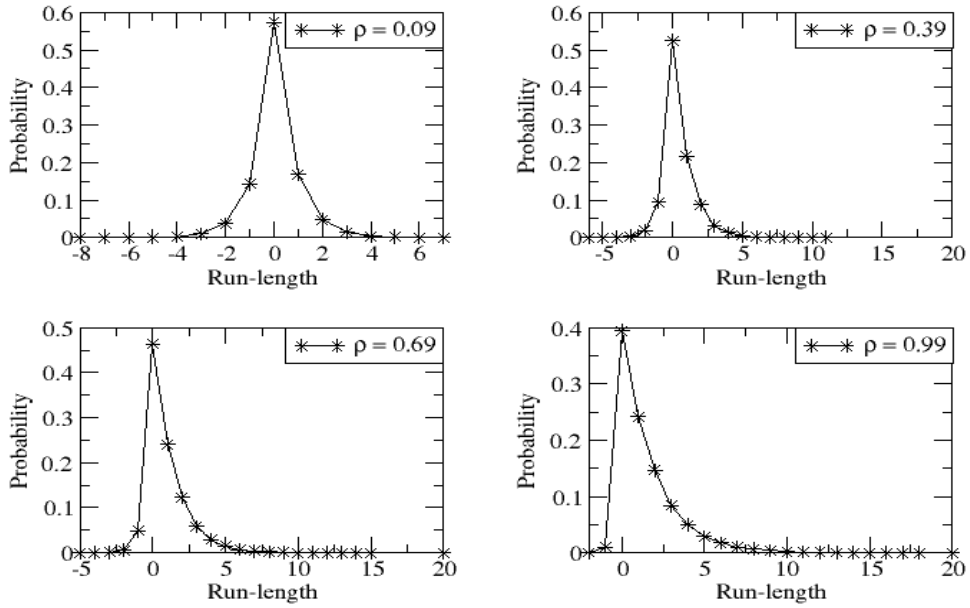

Figure 3.14: Run−length distribution with ATP−intake probability $p = 0.54$.

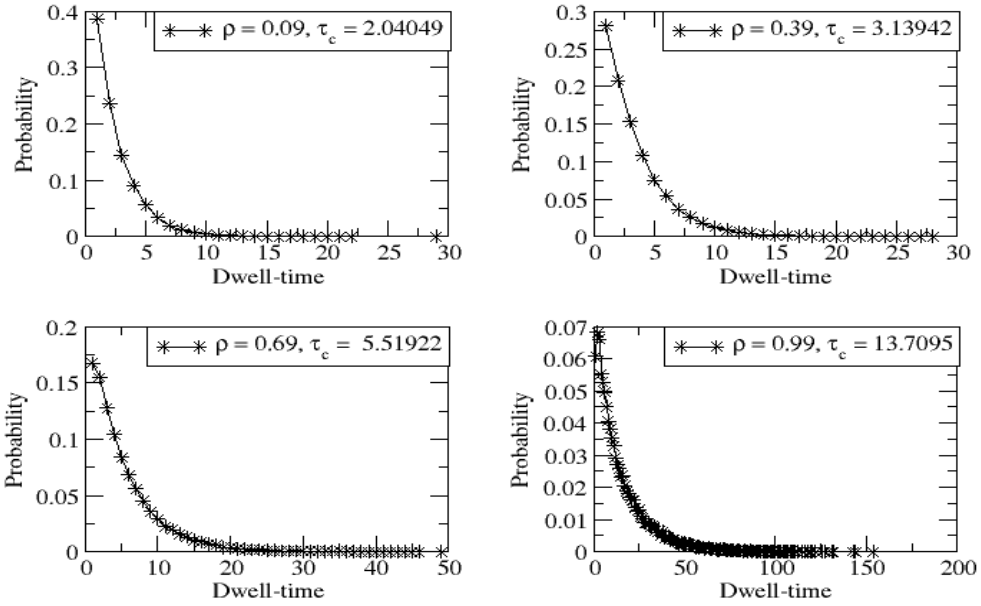

Figure 3.15: Dwell−time distribution with ATP−intake probability $p = 0.99$.

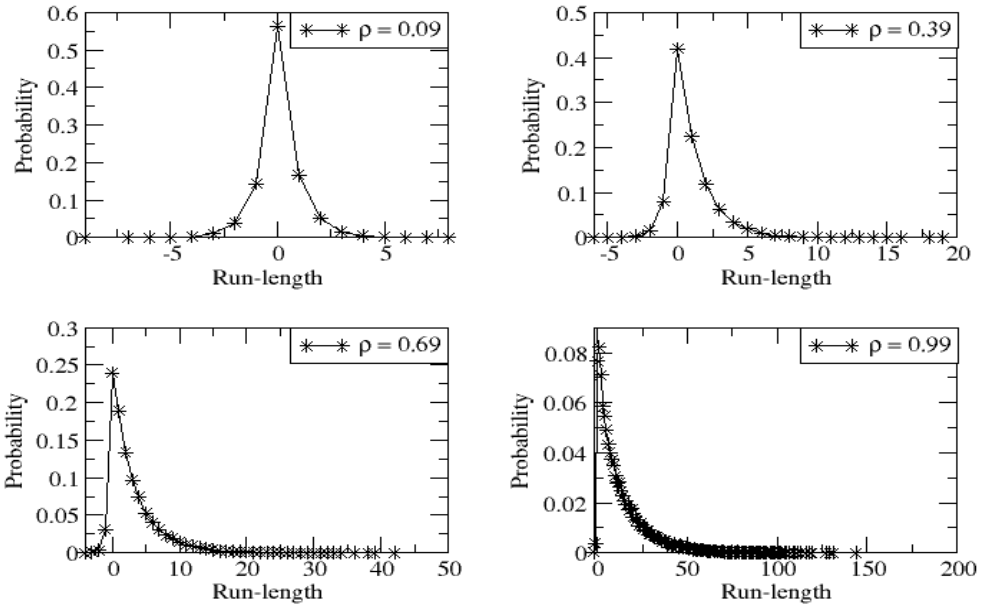

Figure 3.16: Run−length distribution with ATP−intake probability $p = 0.99$.

3.2 Motor proteins transporting a common cargo

Using the bead−spring model for collective motors, we studied mean square displacement dependence of interacting motor proteins transporting cooperatively a common cargo on motor proteins number N, motor proteins mean spacing q, and spring stiffness k (see Fig. 2.2). In our simulation, we used 15, 5, and 0 for l_1, l_2, and w_j respectively.

3.2.1 Mean square displacement (MSD) dependence on motor proteins number (N)

We studied mean square displacement dependence on motor proteins number N with motor proteins mean spacing $q = 50$, and spring stiffness $k = 0.1$. As seen from Fig. 3.17, the mean square displacement (MSD) is a linear function of Monte Carlo time step (MCS) after a transient, and the slope decreases with increasing motor proteins number N. This is because the exclusion interaction comes into play: no two motor proteins occupy the same lattice point.

3.2.2 Mean square displacement (MSD) dependence on motor proteins mean spacing (q)

Figs. 3.18 and 3.19 show, as we increase the mean spacing between adjacent motor proteins q, the slope of the mean square displacement (MSD) also increases. This is also expected to happen because the exclusion interaction gets weaker as the mean spacing q gets wider.

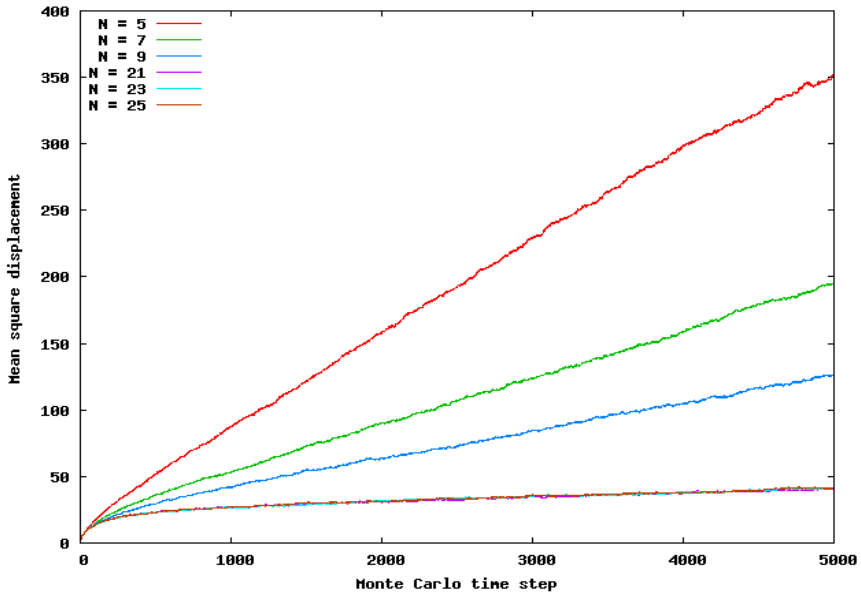

Figure 3.17: Mean square displacement (MSD) vs. Monte Carlo time step (MCS) for different motor proteins number N. We did the plot for mean motor spacing $q = 50$, spring stiffness $k = 0.1$, and saw−tooth potential height $H = 1.0$. The plot is for motor protein $i = \frac{N-1}{2}$ (see Fig. 2.2).

3.2.3 Mean square displacement (MSD) dependence on spring stiffness (k)

As seen from Figs. 3.20 and 3.21, the mean square displacement (MSD) and the spring stiffness k have inverse relation: the slope of the mean square displacement (MSD) decreases as we increase the spring stiffness k. For high spring stiffness k, the motor proteins are highly coupled.

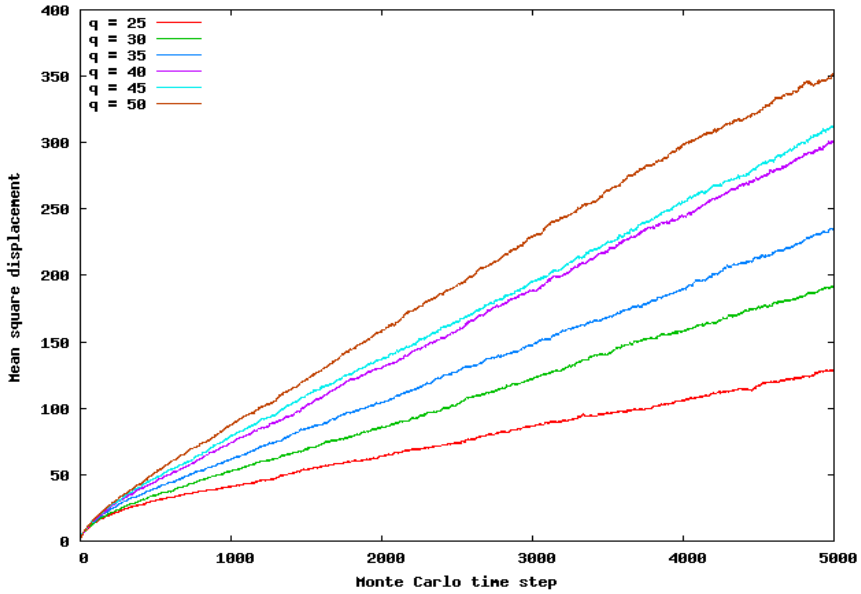

Figure 3.18: Mean square displacement (MSD) vs Monte Carlo time step (MCS) for different motor mean spacing q. We did the plot for motor proteins number $N = 5$, spring stiffness $k = 0.1$, and saw−tooth potential height $H = 1.0$. The plot is for motor protein $i = \frac{N-1}{2}$.

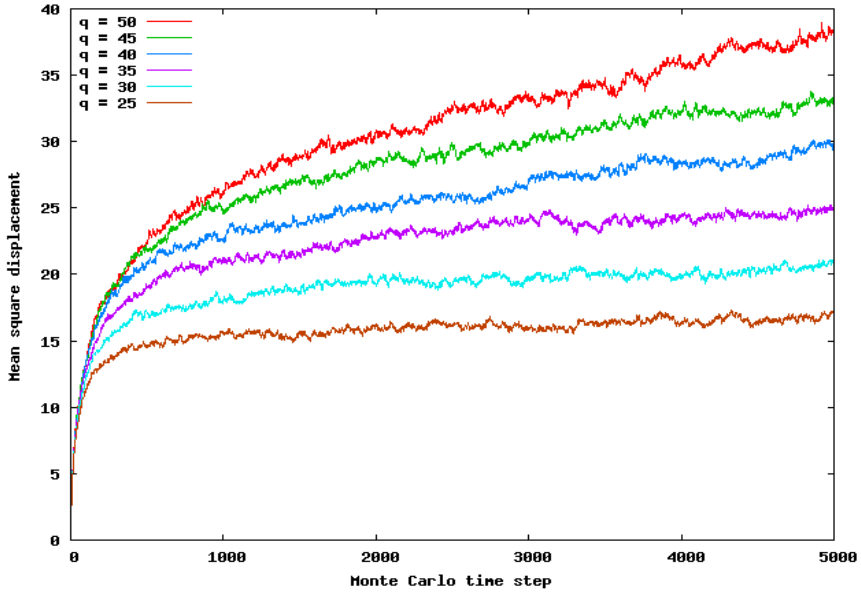

Figure 3.19: Mean square displacement (MSD) vs Monte Carlo time step (MCS) for different motor mean spacing q. We did the plot for motor proteins number $N = 25$, spring stiffness $k = 0.1$, and saw−tooth potential height $H = 1.0$. The plot is for motor protein $i = \frac{N-1}{2}$.

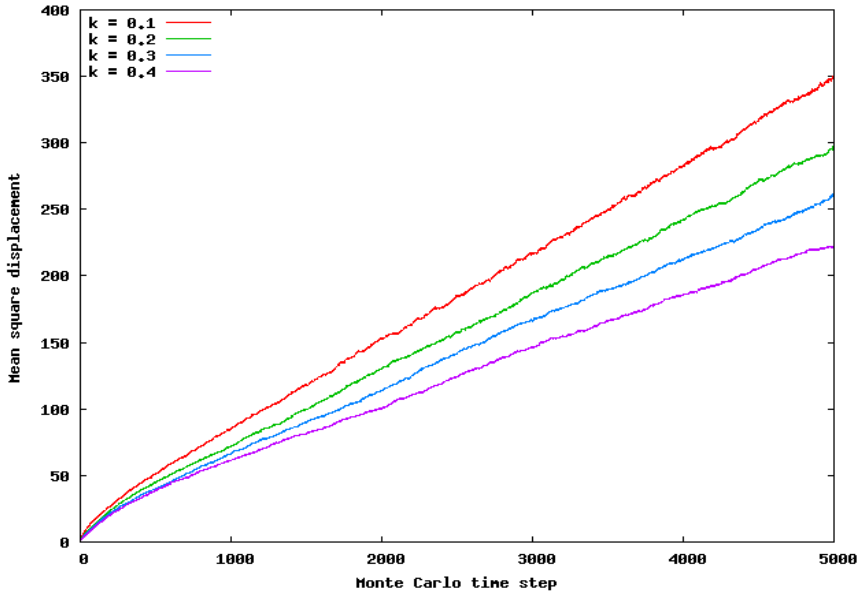

Figure 3.20: Mean square displacement (MSD) vs. Monte Carlo time step (MCS) for different spring stiffness (k) with motor proteins number $N = 5$, mean spacing $q = 50$, and saw−tooth potential height $H = 1.0$. The plot is for motor protein $i = \frac{N-1}{2}$.

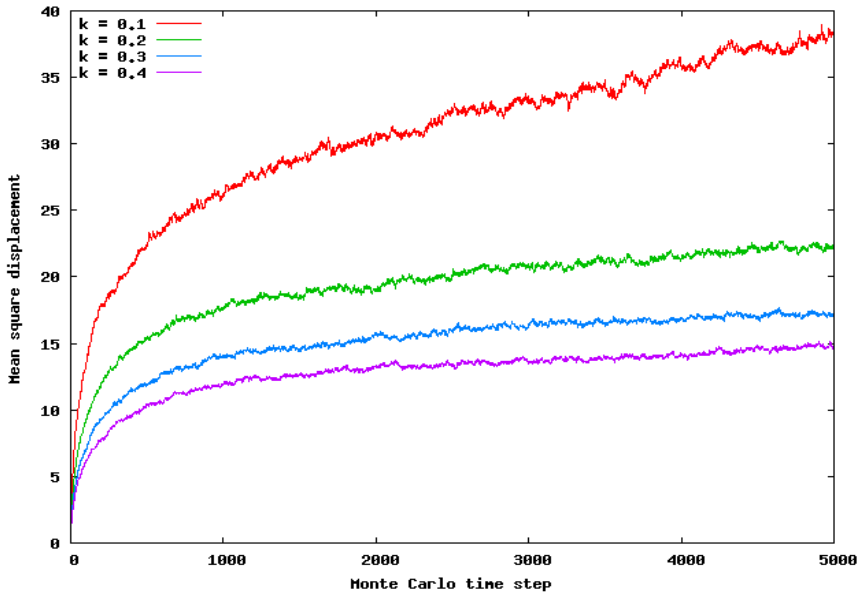

Figure 3.21: Mean square displacement (MSD) vs. Monte Carlo time step (MCS) for different spring stiffness (k) with motor proteins number $N = 25$, mean spacing $q = 50$, and saw−tooth potential height $H = 1.0$. The plot is for motor protein $i = \frac{N-1}{2}$.

Chapter 4

Summary and Conclusion

In this simulation study, we tried to study the dynamics of non−interacting motor proteins each transporting a cargo and interacting motor proteins transporting cooperatively a common cargo; though our study needs more investigations, especially for the collective motor proteins case.

We first studied the processivity of non−interacting motor proteins each transporting a cargo. To understand their processivity, we calculate Hurst exponents, forward/backward step ratios, dwell−time and run−length distributions of a motor protein for different ATP concentrations ρ and ATP−intake probabilities p. Our simulation shows that processive motor proteins which are characterized by high ATP−intake probabilities p can move hundreds of steps, which is seen in single−molecule experiments.

We then studied the collective effect of motor proteins working together using our bead−spring model. We investigate the dependence of mean square displacement (MSD) on motor proteins number N, mean spacing between adjacent motor proteins q, and spring stiffness k. The results show that the slope of the mean square displacement (MSD) increases with increasing mean spacing between adjacent motor proteins q, and decreases with increasing motor proteins number N and spring stiffness k.

Bibliography

[1] H. Lodish, *Molecular cell biology 6th ed.* (New York: W. H. Freeman, 2008).

[2] J. Howard, *Mechanics of motor proteins and cytoskeleton* (Sunderland, MA: Sinauer Associates, 2001).

[3] R. D. Vale, Trends Cell Biol. **9**, M38 (1999).

[4] A. B. Kolomeisky, M. E. Fisher, Annu. Rev. Phys. Chem. **58**, 675 (2007).

[5] S. Klumpp, R. Lipowsky, Proc. Natl. Acad. Sci. U.S.A. **102**, 17284 (2005).

[6] J. R. Kardon and R. D. Vale, Nature Rev. Molec. Cell Biol. **10**, 854 (2009).

[7] S. A. Endow, Nature Rev. Cell Biol. **1**, E163 (1999).

[8] F. Kozielski, S. Sack, A. Marx, M. Thormählen, E. Schönbrunn, V. Biou, A. Thompson, E.M. Mandelkow, E. Mandelkow, Cell (Cambridge, Mass.) **91**, 985 (1997).

[9] A. P. Carter, C. Cho, L. Jin, R. D. Vale, Science **331**, 1159 (2011).

[10] A. Houdusse and A. P. Carter, Cell **136**, 395 (2009).

[11] C. Veigel and C. F. Schmidt, Nature Rev. Molec. Cell Biol. **12**, 163 (2011).

[12] Y. Ishii and T. Yanagida, Single Mol. **1**, 5 (2000).

[13] F. Ritort, J. Phys. Condens. Matter **18**, R531 (2006).

[14] W. O. Hancock, J. Howard, Proc. Natl. Acad. Sci. U.S.A. **96**, 13147 (1999).

[15] A. Gennerich and R. D. Vale, Curr. Opin. Cell Biol. **21(1)**, 59 (2009).

[16] D. Gillo, B. Gur, A. Bernheim−Groswasser and O. Farago, Phys. Rev. E **80**, 021929 (2009).

[17] C. Leduc, F. Ruhnow, J. Howard, S. Diez, Proc. Natl. Acad. Sci. U.S.A. **104**, 10847 (2007).

[18] F. Julicher, A. Ajdari, and J. Prost, Rev. Mod. Phys. **69(4)**, 1269 (1997).

[19] M. Badoual, F. Jülicher, and J. Prost, Proc. Natl. Acad. Sci. U.S.A. **99**, 6696 (2002).

[20] R. D. Vale, Cell **112**, 467 (2003).

[21] D. W. Heermann, *Computer Simulation Methods in Theortical Physics 2nd ed.* (Springer−Verlag Berlin Heidelberg, 1990).

[22] M. P. Allen, D. J. Tildesley, *Computer Simulation of liquids* (New York: Oxfored University Press, 1991).

[23] D. P. Landau, K. Binder, *A Guide to Monte Carlo Simulations in Statistical Physics 2nd ed.* (New York: Cambridge University Press, 2005).

[24] N. Metropolis, S. Ulam, American Statistical Association Journal **44**, 335 (1949).

[25] R. Lipowsky, S. Klumpp, and T. M. Nieuwenhuizen, Phys. Rev. Lett. **87**, 108101 (2001).

[26] N. J. Carter and R. A. Cross, Nature **435**, 308 (2005).

[27] T. M. Nieuwenhuizen, S. Klumpp and R. Lipowsky, Europhysics. Lett. **58(3)**, 468 (2002).

[28] L. Bruno, M. Salierno, D. E. Wetzler, M. A. Desposito, V. Levi, PLoS ONE **6(4)**, e18332 (2011).

[29] A. G. Hendricks and B. I. Epureanu, Phys. Rev. E **79**, 031929 (2009).

[30] C. W. Wolgemuth and S. X. Sun, Phys. Rev. Lett. **97**, 248101 (2006).

[31] I. Schwaiger, C. Sattler, D. R. Hostetter and M. Rief, Nature Materials **1**, 232 (2002).

[32] R. P. Erickson, Z. Jia, S. P. Gross, C. C. Yu, PLoS Computational Biology **7(5)**, e1002032 (2011).

[33] N. Metropolis, A. W. Rosenbluth, M. N. Rosenbluth, and A. H. Teller, J. Chem. Phys. **21**, 1087 (1953).

[34] O. Campàs. Y. Kafri, K. B. Zeldovich, J. Casademunt, and J.−F. Joanny, Phys. Rev. Lett. **97**, 038101 (2006).

Declaration

This thesis is my original work, has not been presented for a degree in any other University and that all the sources of material used for the thesis have been dully acknowledged.

Name: Asmamaw Asrat

Signature:

Place and time of submission: Addis Ababa University, July 2011

This thesis has been submitted for examination with my approval as University advisor.

Name: Dr. Tatek Yergou

Signature: